Biochimica et Biophysica Acta 1848 (2015) 408–416

Contents lists available at ScienceDirect

Biochimica et Biophysica Acta

journal homepage: www.elsevier.com/locate/bbamem

The p10 FAST protein fusion peptide functions as a cystine noose to induce cholesterol-dependent liposome fusion without liposome tubulation

Tim Key [a], Muzaddid Sarker [a,b], Roberto de Antueno [a], Jan K. Rainey [b,c,*], Roy Duncan [a,b,d,**]

[a] Department of Microbiology & Immunology, Dalhousie University, Halifax, Nova Scotia B3H 4R2, Canada
[b] Department of Biochemistry & Molecular Biology, Dalhousie University, Halifax, Nova Scotia B3H 4R2, Canada
[c] Department of Chemistry, Dalhousie University, Halifax, Nova Scotia B3H 4R2, Canada
[d] Department of Pediatrics, Dalhousie University, Halifax, Nova Scotia B3H 4R2, Canada

ARTICLE INFO

Article history:
Received 7 June 2014
Received in revised form 5 October 2014
Accepted 15 October 2014
Available online 23 October 2014

Keywords:
Fusion peptide
Membrane fusion
Viral fusion peptides
Liposome fusion

ABSTRACT

The reovirus p10 fusion-associated small transmembrane (FAST) proteins are the smallest known membrane fusion proteins, and evolved specifically to mediate cell–cell, rather than virus–cell, membrane fusion. The 36–40-residue ectodomains of avian reovirus (ARV) and Nelson Bay reovirus (NBV) p10 contain an essential intramolecular disulfide bond required for both cell–cell fusion and lipid mixing between liposomes. To more clearly define the functional, biochemical and biophysical features of this novel fusion peptide, synthetic peptides representing the p10 ectodomains of ARV and NBV were analyzed by solution-state NMR spectroscopy, circular dichroism spectroscopy, fluorescence spectroscopy-based hydrophobicity analysis, and liposome binding and fusion assays. Results indicate that disulfide bond formation promotes exposure of hydrophobic residues, as indicated by bis-ANS binding and time-dependent peptide aggregation under aqueous conditions, implying the disulfide bond creates a small, geometrically constrained, cystine noose. Noose formation is required for peptide partitioning into liposome membranes and liposome lipid mixing, and electron microscopy revealed that liposome–liposome fusion occurs in the absence of liposome tubulation. In addition, p10 fusion peptide activity, but not membrane partitioning, is dependent on membrane cholesterol.

1. Introduction

Fusion of two cell membranes is an important step in many essential biological processes, such as fertilization, formation of the syncytiotrophoblast layer of the placenta, myoblast fusion during muscle development, and formation of osteoclasts for bone resorption [1]. Membrane fusion is also an essential step in the infection of host cells by enveloped viruses, such as HIV and influenza [2]. Such membrane merger events are energetically unfavorable processes and require protein fusogens to mediate fusion of biological membranes under physiological conditions. In the case of enveloped virus fusion proteins, the process involves triggered, complex structural rearrangements of the fusion proteins. These conformational changes expose a hydrophobic sequence known as the fusion peptide (FP), which is normally sequestered from solvent within the pre-fusion structure. Formation of an extended intermediate projects the FP toward the target membrane for membrane insertion. Folding back of this extended intermediate into a compact trimeric hairpin structure is believed to provide energy to pull the apposed membranes together and drive membrane merger [3]. Exactly how membrane fusion proteins mediate the actual merger of membranes, and the precise role of FPs in this process, is still unclear.

While extensive structural remodeling of enveloped virus fusion proteins is clearly a key event in the fusion process, it seems likely that FPs serve a greater role in promoting membrane merger than just serving as membrane anchors [4]. There are two general classes of enveloped virus FPs. The first are N-terminal FPs in proteins such as influenza virus hemagglutinin (HA) and HIV gp41, which form amphipathic α-helices that are frequently kinked or in a helical hairpin conformation, exposing hydrophobic faces for membrane insertion [5–7]. The

Abbreviations: Δδ, secondary chemical shift; ARV, avian reovirus; bis-ANS, 4,4′-dianilino-1,1′-binaphthyl-5,5′-disulfonic acid; Chol, cholesterol; CM, conserved motif; DTT, dithiothreitol; DMSO, dimethyl sulfoxide; DOPC, 2-dioleoyl-*sn*-glycero-3-phosphocholine; DPC, dodecylphosphocholine; FAST, fusion-associated small transmembrane; FP, fusion peptide; HFIP, 1,1,1,3,3,3-hexafluoro-2-propanol; NBD-DOPE, 1,2-dioleoyl-*sn*-glycero-3-phosphoethanolamine-N-(7-nitro-2-1,3-benzoxadiazol-4-yl); NBV, Nelson Bay reovirus; p10ecto, p10 ectodomain peptide; p10ectoTr, truncated p10 ectodomain peptide; NOESY, nuclear Overhauser enhancement spectroscopy; Rho-DOPE, 1,2-dioleoyl-*sn*-glycero-3-phosphoethanolamine-N-4(lissamine rhodamine B sulfonyl); Sph, sphingomyelin; TCEP, tris(2-carboxyethyl)phosphine; TOCSY, total correlation spectroscopy.

* Correspondence to: J. Rainey, Department of Biochemistry & Molecular Biology, Dalhousie University, Halifax, Nova Scotia B3H 4R2, Canada. Tel.: +1 902 494 4632.
** Correspondence to: R. Duncan, Department of Microbiology & Immunology, Dalhousie University, Halifax, Nova Scotia B3H 4R2, Canada. Tel.: +1 902 494 6770.
E-mail addresses: jan.rainey@dal.ca (J.K. Rainey), roy.duncan@dal.ca (R. Duncan).

http://dx.doi.org/10.1016/j.bbamem.2014.10.020
0005-2736/

second class are referred to as fusion loops, and are present in proteins such as dengue virus E1 and Ebolavirus gp2 [8,9]. These loops are flanked by elongated, anti-parallel β-strands and expose hydrophobic residues at the apex of the loop for membrane insertion. The prevailing view is that FPs shallowly insert into the outer leaflet of membrane bilayers, inducing membrane bending that results in formation of a dimple. Dimple formation would promote close membrane apposition, with membrane bending stresses in the highly curved lipidic cap of the dimple being relieved by membrane merger [10]. Support for this model of FP function derives from studies of cellular proteins involved in vesicle fusion. For example, shallow insertion of an amphipathic helix in the endophilin N-BAR domain or hydrophobic loops in the C2 domains of synaptotagmin and Doc2b proteins induce extensive membrane curvature resulting in liposome tubulation and generation of highly fusogenic lipidic end caps on these tubules [11–15]. Whether viral FPs induce liposome fusion via a similar tubulation mechanism has not been determined.

In addition to enveloped viruses, a single family of nonenveloped viruses also encodes membrane fusion proteins. The fusion-associated small transmembrane (FAST) proteins are encoded by the fusogenic *Aquareoviruses* and *Orthoreoviruses*, two genera in the family *Reoviridae*, a large diverse group of nonenveloped viruses with segmented, dsRNA genomes [16]. FAST proteins are nonstructural viral proteins expressed inside virus-infected cells, where they traffic to the plasma membrane to induce cell–cell membrane fusion and syncytium formation [17]. All FAST proteins are integral membrane proteins, with a single transmembrane domain separating very small (~20–40 residues) N-terminal ectodomains from equal-sized or considerably larger C-terminal cytoplasmic endodomains [18–23]. The homologous p10 FAST proteins of avian (ARV) and Nelson Bay (NBV) orthoreoviruses, and the unrelated p14 and p15 FAST proteins of reptilian (RRV) and baboon orthoreoviruses, respectively, all contain motifs in their small ectodomains that share features with canonical viral FPs [17]. These FP motifs are essential for cell–cell fusion, and synthetic peptides based on these motifs induce liposome–liposome lipid mixing. Structurally, these motifs differ dramatically from each other, and from enveloped virus FPs. An intramolecular disulfide bond in p10 creates an 11-residue cystine loop FP, the p14 FP contains a 7-residue proline-hinged loop, while the 19-residue p15 ectodomain FP comprises a polyproline type II helix flanked by short, amphiphilic, unstructured regions [24–26]. Aside from being essential for cell–cell fusion and inducing lipid mixing between liposomes, these atypical FAST protein FPs remain poorly characterized.

At 95–98 residues in size, the p10 FAST proteins encoded by avian and bat reoviruses are the smallest known viral or cellular membrane fusion proteins. We recently reported the presence of a cystine loop FP in ARV and NBV p10, and showed stringent sequence constraints within and flanking the cystine loop affect formation of the intramolecular disulfide bond [27]. Specific features of the p10 cystine loop are quite distinct from enveloped virus fusion loops. For example, the enveloped virus fusion loops are located at the tips of disulfide-stabilized structures comprising anti-parallel β-strands [9,28] or in order-turn-order structures [29,30]. In some cases, such as Ebola virus gp2, the fusion loop is actually partly helical [31,32]. Enveloped virus FPs that function as fusion loops are therefore components of larger structures, and the role of disulfide bonds is to stabilize the overall fusion domain rather than the FP directly. In contrast, the p10 ectodomain is only 36–40 residues in size, and the 11-residue fusion loop is self-contained within a 15–19 residue sequence that is solely required for formation of the cystine loop FP [27]. We now show that formation of the p10 intramolecular disulfide bond forces solvent exposure of hydrophobic residues, suggesting the cystine loop functions as a cystine noose [33]. Cystine noose formation is required for membrane partitioning, structural transitions and fusion activity. Additionally, we demonstrate that p10-induced liposome-liposome fusion occurs in the absence of liposome tubulation, and that cholesterol is required for the post-binding lipid mixing stage of p10-mediated membrane fusion.

2. Materials and methods

2.1. Synthetic peptides

Peptides corresponding to the ectodomain (residues 1–40) of the ARV p10 protein (ARV p10ecto) were synthesized by Genscript to contain an intramolecular disulfide bond between Cys9 and Cys21. Peptides corresponding to a partially truncated (residues 4–36) ARV p10 ectodomain (p10ectoTr) and to the NBV p10 ectodomain (residues 1–35, NBV p10ecto) were synthesized by United Peptide to contain a similar intramolecular disulfide bond. A similar NBV p10ecto peptide containing a Ser substitution of Cys5 (NBV p10C5ecto) to prevent formation of the disulfide bond was also synthesized by United Peptide. All peptides were purified to 95% purity by HPLC and confirmed by mass spectrometry.

2.2. Hydrophobicity and aggregation analysis

Hydrophobicity predictions were performed with Protscale on the ExPASy server, using a sliding window average of 5 residues. Relative hydrophobicity was measured in aqueous conditions (10 mM $NaPO_4$, 100 mM NaF, pH 7.4) using 4.7 μM 4,4′-dianilino-1,1′-binaphthyl-5,5′-disulfonic acid (bis-ANS, Invitrogen) and 80 μM of a given p10 ectodomain peptide with and without 20 mM tris(2-carboxyethyl)phosphine (TCEP). Steady-state fluorescence spectroscopy was performed using a Varian Cary Eclipse spectrofluorometer at 35 °C in a 3 mm quartz cuvette (Varian), with excitation and emission slit widths of 5 nm. Emission spectra were measured from 460 to 600 nm with an excitation wavelength of 360 nm. Time-dependent aggregation of the p10ecto peptide (0.5 mM), in aqueous conditions (10 mM $NaPO_4$, 100 mM NaF, pH 7.4) with and without 5 mM dithiothreitol (DTT), was followed by OD350 measurements using a Varian Cary 50 UV/Vis spectrophotometer. All spectra were background subtracted. Bis-ANS experiments were repeated in quadruplicate, while peptide aggregation experiments were performed in triplicate.

2.3. Solution-state nuclear magnetic resonance (NMR) spectroscopy

Solution-state NMR experiments were performed on the p10ectoTr peptide in the organic solvents dimethyl sulfoxide (DMSO-d_6) and hexafluoro-2-propanol (HFIP-d_2), and in the sodium dodecylsulfate (SDS-d_{25}) and dodecylphosphocholine (DPC-d_{38}) membrane-micellar mimetic environments. Organic solvent samples were prepared by dissolving the peptide (~0.5 mM) in 100% DMSO-d_6 or 50% HFIP-d_2 plus 40% H_2O and 10% D_2O. Micelle samples were prepared by dissolving the peptide in SDS-d_{25} or DPC-d_{38} (150 mM) in 90% H_2O and 10% D_2O, and adjusting the pH to 5.0. The HFIP, SDS and DPC samples also contained 0.5 mM sodium 2,2-dimethyl-2-silapentane-5-sulfonate (DSS) and 0.2 mM sodium azide. The SDS and DPC samples were buffered with 20 mM sodium acetate (pH 5.0). NMR data were acquired using a Bruker Avance III 700 MHz spectrometer equipped with a 5 mm triple-resonance inverse cryoprobe and processed using Bruker Topspin 3.1. 1D ^1H, 2D ^1H–^1H total correlation spectroscopy (TOCSY; number of scans 16, size of fid 2048/512 in F2(^1H)/F1(^1H), sweep width 12/12 ppm in F2/F1, recycle delay 2 s, mixing time 60/120 ms, DIPSI2 isotropic mixing sequence) and 2D ^1H–^1H nuclear Overhauser enhancement spectroscopy (NOESY; number of scans 16, size of fid 2048/512 in F2(^1H)/F1(^1H), sweep width 12/12 ppm in F2/F1, recycle delay 2 s, mixing time 200–400 ms) spectra were acquired for the p10ectoTr peptide under all four solvent conditions at 22 and 37 °C. Spectra collected in HFIP, SDS and DPC were referenced to internal DSS at 0 ppm. Spectra collected in DMSO were indirectly referenced to 0 ppm for aqueous DSS using the intermediate trimethylsilane (TMS) shift. Spin system assignment was performed, to the extent possible, in Sparky 3.110 (Goddard, T.D., and Kneller, D.G. Sparky 3, University of California, San Francisco). Secondary chemical shifts ($\Delta\delta$) for H^α resonances of unambiguously identified residues were calculated by

subtracting random coil chemical shifts for peptides of sequence GGXAGG measured in DMSO [34] from those measured in p10ectoTr.

2.4. Circular dichroism (CD) spectropolarimetry

Far-UV (260–185 nm) CD spectra of p10ecto peptide were recorded using a Jasco J-810 spectropolarimeter (Easton, MD) at 35 °C using 0.01 cm quartz cuvettes (Hellma, Müllheim, Germany). Spectra were obtained using 0.05 mg ARV p10 ectodomain peptide, with or without reduction by 5 mM DTT, in aqueous solution (10 mM $NaPO_4$, 100 mM NaF) or in the presence of 100 mM liposomes (40:30:20:10 molar ratio of 1,2-dioleoyl-*sn*-glycero-3-phosphocholine [DOPC]:1,2-dioleoyl-*sn*-glycero-3-phosphoethanolamine [DOPE]:cholesterol [Chol]: sphingomylein [Sph]; 100 nm diameter). Six replicate spectra were acquired in 0.1 nm steps and the raw data, averaged, blank subtracted, converted to mean residue ellipticity [θ] and averaged using a weighted 3 nm sliding-window.

2.5. Lipid mixing assay

A fluorescence resonance energy transfer (FRET)-based mixing assay was employed to monitor the lipid-mixing potential of synthetic p10 ectodomain peptides [35]. Liposomes composed of a constant 30 mol% DOPE and the indicated amounts of DOPC, Chol and Sph (Avanti Polar Lipids) in 10 mM $NaPO_4$, 100 mM NaF, pH 7.4, were prepared and extruded to 100 nm as previously described [26]. A fluorescently-labeled liposome population was similarly prepared to contain 2 mol% each of 1,2-dioleoyl-*sn*-glycero-3-phosphoethanolamine-N-(7-nitro-2-1,3-benzoxadiazol-4-yl) (NBD-DOPE) and 1,2-dioleoyl-*sn*-glycero-3-phosphoethanolamine-N-4(lissamine rhodamine B sulfonyl) (Rho-DOPE). Non-labeled and labeled liposomes at a final concentration of 100 μM were incubated at 37 °C in a 9:1 ratio prior to addition of p10ecto synthetic peptide (10 μM) or buffer only control (10 mM $NaPO_4$, 100 mM NaF, pH 7.4). Fluorescence emission was recorded for up to ten minutes at 37 °C using an excitation wavelength of 460 nm and an emission wavelength of 535 nm on a Varian Cary Eclipse fluorescent spectrophotometer. A third liposome population containing 0.2 mol% each of NBD-DOPE and Rho-DOPE was measured identically to determine the theoretical maximum (F_{MAX}) level of lipid mixing. The percent lipid mixing was calculated as previously shown [26]. All experiments were performed in quadruplicate.

2.6. Peptide partitioning into liposome membranes

Liposomes (100 nm diameter) of a constant 30% DOPE and 10% Sph composition, containing a given proportion of Chol and the corresponding proportion of DOPC, were incubated in a 1:10 ratio with p10ecto peptide (125 μM) in 250 μL of 10 mM $NaPO_4$, 100 mM NaF, pH 7.4, with or without 5 mM DTT. Samples were mixed with an equivalent volume of 60% sucrose, then successively overlaid with 800 μL of 20% sucrose and 100 μL of buffer. Samples were centrifuged at 50 K rpm for 45 min at 4 °C in a Beckman SW60 Ti rotor (256,000 ×*g*), the liposome-containing fraction at the 20%–0% sucrose interface was harvested and mixed with 2× protein sample buffer (20%SDS, glycerol, Tris–HCl, pH 6.8), and p10ecto peptide detected by tricine SDS-PAGE and silver staining.

2.7. Electron microscopy

Liposomes (100 nm diameter) composed of 40:30:20:10 of DOPC: DOPE:Chol:Sph (100 μM) were incubated with buffer alone (10 mM $NaPO_4$, 100 mM NaF, pH 7.4), ARV p10 or NBV p10 ectodomain peptides (10 μM) for 5 min at 37 °C. Samples were settled on to Formvar/carbon coated grids, stained with 2% uranyl acetate, and visualized on a JEOL JEM 1230 transmission electron microscope. Liposome sizes were determined by measuring diameters of at least 900 liposomes present in five random fields from two separate experiments at 50–80,000× magnification using ImageJ. Liposome sizes were binned and presented as percent liposomes in each bin size, or as percent total liposome volume in each bin size, calculated by dividing the sum of liposome volumes in each bin by the total volume of liposomes.

3. Results and discussion

3.1. Cystine loop formation forces solvent exposure of hydrophobic residues and causes aggregation of the p10 ectodomain

The NBV and ARV p10 ectodomains are 36 or 40 residues in length, respectively (Fig. 1A). The C-terminal 13 residues of each ectodomain contain a 9-residue conserved motif (CM), which is present in all p10 proteins from both avian and pteropine reoviruses and is responsible for cholesterol-dependent p10 multimerization [27]. The cystine loop FP is N-terminal to the CM, spanning Cys9–Cys21 in ARV p10 and Cys5–17 in NBV p10. Loop formation is influenced by residues immediately flanking the two cysteines but is unaffected by the membrane-proximal multimerization motif [27]. Seven of the eleven amino acids in the p10 cystine loops are hydrophobic or apolar, with NBV p10 being slightly more hydrophobic than ARV p10 (Fig. 1A). Both proteins contain a conserved Val-Phe dipeptide at the apex of their loops. Polar residues in the loop are tolerant of substitution, while hydrophobic residues are intolerant of even minor changes in hydrophobicity, with a clear preference for Phe or Trp at the apex of the loop [36,37]. We previously speculated that the cystine loop might function as a cystine noose, a short disulfide-stabilized loop structure [33], to force solvent exposure of hydrophobic residues in the p10 FP [24].

To explore whether the p10 FP functions as a cystine noose, a synthetic peptide representing the 40-residue ARV p10 ectodomain (Fig. 1A) was commercially synthesized to include the essential intramolecular disulfide bond between Cys9 and Cys21, which creates the essential cystine loop [24]. A similar peptide of the 36-residue NBV p10 ectodomain (Fig. 1A) was also synthesized containing an intramolecular disulfide bond. The hydrophobicity of these peptides was directly assessed using bis-ANS. Anilinonaphthalene sulfonates (ANS) are nonfluorescent in polar solvents but exhibit strong fluorescence when bound to apolar molecules, and are commonly employed as probes sensitive to solvent exposure of hydrophobic amino acids [38]. As shown (Fig. 1B), the loop-containing ARV and NBV peptides both induced bis-ANS fluorescence, which was substantially decreased when the disulfide bond was reduced by TCEP. In addition, the presence of more hydrophobic residues within the NBV loop (Fig. 1A) correlated with increased bis-ANS fluorescence induced by the NBV peptide (Fig. 1B). To ensure the reducing agent had no intrinsic effect on bis-ANS fluorescence, the NBV p10ecto was compared to the same peptide containing a Ser substitution of Cys5 (NBV p10C5ecto). The mutant peptide in the absence or presence of TCEP displayed a similar reduction in bis-ANS fluorescence as the reduced parental peptide (Fig. 1C). The disulfide bond therefore substantially increases the hydrophobicity of the ARV and NBV FPs.

Although the ARV p10ecto peptide was soluble at a concentration of 0.5 mM under aqueous conditions (conditions compatible with NMR analysis), measurement of light scattering at 350 nm demonstrated time-dependent peptide aggregation with a lag phase of ~15 h before a rapid increase in scattering (Fig. 1D). A similar situation occurred with a slightly truncated version of the ARV p10 ectodomain peptide (p10ectoTr), missing the N-terminal Met-Leu-Arg and C-terminal Ser-Ile-Ile-Ala residues, as well as with synthetic peptides of the NBV p10 ectodomain (data not shown). Disruption of the intramolecular disulfide bond with 5 mM DTT prevented aggregation in aqueous conditions (Fig. 1D). The long lag phase prior to peptide aggregation suggests that simple hydrophobic interactions alone may not account for peptide aggregation at concentrations suitable for NMR. Peptide aggregation is influenced by peptide hydrophobicity, secondary structure propensity, surface charge density, and monomer concentrations [39,40]. Time scales for aggregation can range from μs for proteins such as the human islet

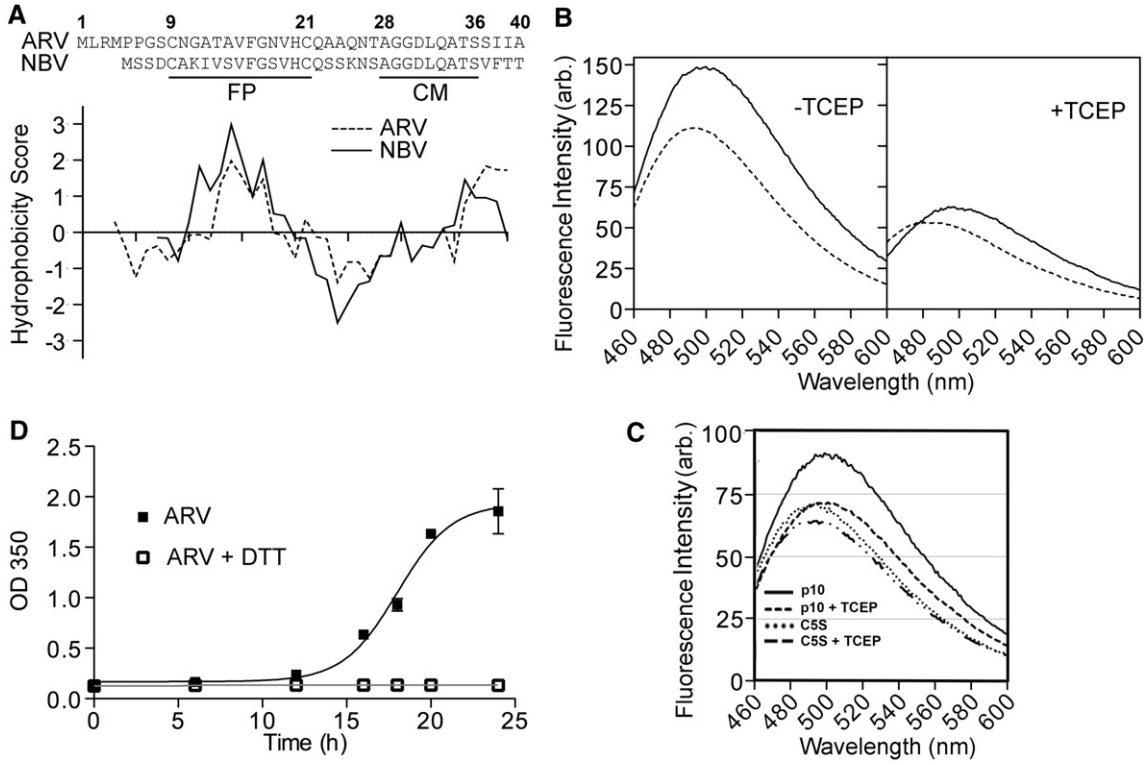

Fig. 1. The p10 disulfide bond forces exposure of hydrophobic residues. (A) Sequence alignment of the ARV and NBV p10 ectodomains (top), indicating the locations of the cystine loop fusion peptide (FP) and conserved motif (CM). Numbers indicate residue positions in the ARV sequence. Predicted hydrophobicity of linear ARV and NBV p10 ectodomains (bottom) based on Kyte and Doolittle hydrophobicity scale using sliding window averages of 5 residues. (B) Fluorescence emission spectra (λ_{ex} = 360 nm) of bis-ANS (4.7 μM) incubated with NBV (solid lines) or ARV (dashed lines) p10ecto peptides (80 μM) with or without TCEP (5 μM). Values are background-subtracted averages of four replicates. (C) As in panel B, using the NBV p10ecto peptide or the NBV p10C5Secto peptide in the presence or absence of TCEP. (D) OD_{350} measurements of the ARV p10ecto peptide in aqueous conditions over time with and without DTT.

amyloid polypeptide (hIAPP) [41] to minutes and hours for proteins such as the β-amyloid (Aβ) peptide [42]. It is possible that localized "drying" of exposed hydrophobic residues and a concomitant increase in the hydration density around nearby hydrophilic residues delays hydrophobic aggregation of the p10 ectodomain peptide. The sigmoidal aggregation kinetic profile is also consistent with a nucleation-and-growth process, with weak associations between monomeric peptides slowly generating oligomeric nuclei that subsequently grow into higher-order aggregates [43,44].

Regardless of the mechanism of p10 peptide aggregation, the bis-ANS and aggregation results are both consistent with the p10 intramolecular disulfide bond increasing exposure of hydrophobic residues. In addition, previous studies indicated that ARV p10 is rapidly degraded following co-translational insertion into the endoplasmic reticulum membrane compartment [45]. Substitution of either cysteine residue eliminated rapid p10 degradation, as did substitutions that modestly decreased FP hydrophobicity (V15M or V19M), suggesting exposed hydrophobic residues target p10 to the cellular quality control degradation machinery. Most importantly, while decreased FP hydrophobicity increased p10 stability, p10 cell–cell fusion activity was abrogated [45]. Taken together, the present and previous results all suggest the cystine loop functions as a cystine noose, forcing solvent exposure of hydrophobic residues that are required for membrane fusion activity.

3.2. NMR analysis suggests the CM adopts an α-helical structure

Peptide aggregation precluded NMR structural analysis of the cystine loop-containing peptide under aqueous conditions, and structural analysis of the reduced form of the peptide would be of little value since this state of p10 is not able to induce cell–cell fusion [24]. The ARV p10ectoTr peptide was soluble in two different organic solvents, DMSO and HFIP, and in two different membrane-mimetic environments, SDS and DPC micelles. In the course of TOCSY and NOESY analysis by the sequential assignment strategy, it became clear that the NMR spectra exhibited an insufficient number of spin systems to be consistent with the amino acid composition of the peptide in each of the tested conditions (Fig. 2A). Assignment of peaks and identification of spin systems in the p10ectoTr peptide in DMSO, which displayed the maximum number of peaks with reasonable intensities, allowed unambiguous identification of only nine of 33 residues. Interestingly, these residues, Ala28–Ser36, correspond to the CM (Fig. 1A). Spin systems corresponding to the remaining residues were either undetectable in the NMR spectra (15 residues) or could only be ambiguously assigned (9 residues) due to lack of sequential correlations in the NOESY spectrum. The ^{1}H chemical shifts of the assigned amino acids are shown in Supplementary Table S1.

The lack of observable NMR spin systems for regions of the peptide, while other regions were fully observable, indicate the peptide was undergoing intermediate exchange on the NMR time-scale (i.e., on the order of milliseconds [46]) in all examined conditions. Possible sources may be dynamic exchange between monomer and oligomer states, between free and micelle-bound states, and/or conformational exchange of the polypeptide at the millisecond time scale. Similar NMR signal loss has been reported in other systems, for example with the aggregation prone Aβ amyloid and α-synuclein peptides in the presence of small hydrophobic molecules or surfactants [47–49]. The unambiguously assigned amino acids corresponding to the CM indicated this region was not undergoing such conformational exchange in DMSO. Presumably, the observable NMR signals in HFIP, SDS and DPC were also mostly from this region of the peptide.

Negative $\Delta\delta$ values for H^{α} nuclei over all residues in the assigned Ala28–Ser36 range (Fig. 2B) suggest that this region has α-helical propensity [34,50]. Recent studies indicate the CM functions as a p10 multimerization motif [27], and while not conclusive, a helical propensity in the CM is suggestive that p10 assembly into higher order

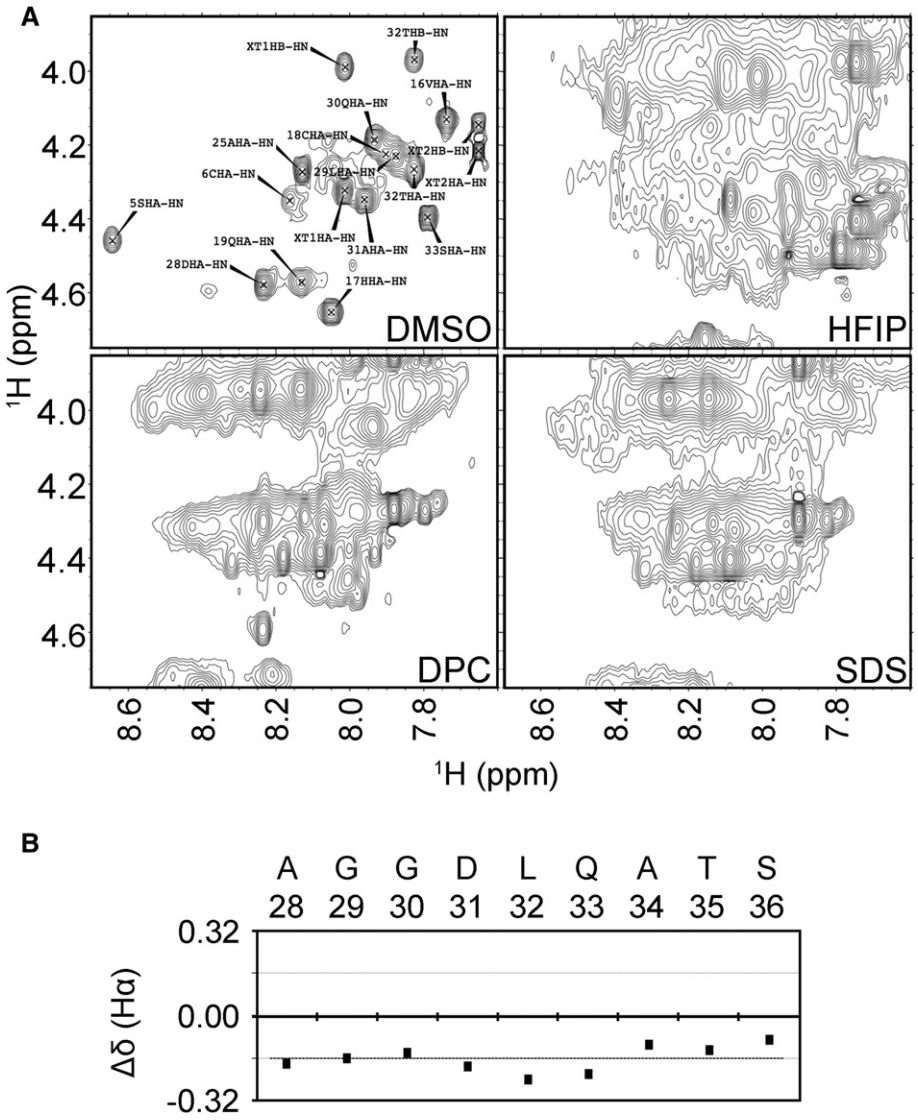

Fig. 2. The p10 ectodomain conserved motif shows α-helical propensity. (A) Hα-HN region of the 2D ^{1}H–^{1}H TOCSY of ARV p10ectoTr in two organic solvents and two micellar environments. Spin systems from only a small proportion of the constituent amino acids, out of the 33 total, are observable. Sequential assignments were performed only under DMSO conditions, where the A28–S36 region was unambiguously assignable. (B) Secondary chemical shifts (Δδ) for Hα resonances, calculated by subtracting the random coil chemical shifts for peptides of sequence GGXAGG determined in DMSO from those of the p10ectoTr A28–S36 amino acids. The negative Δδ values suggest an α-helical propensity for the corresponding residues.

structures may be through complementary helix packing interactions. We note that this potential helical structure might contribute to the aggregation phenomenon, similar to hIAPP where α-helical structures are responsible for weak interactions during the nucleation stage that are subsequently stabilized by hydrophobic interactions to produce high-order aggregates [41]. We also note that, while stable p10 multimer formation requires p10 clustering in cholesterol-rich plasma membrane microdomains [27], associations between exposed hydrophobic residues in the cystine noose might also contribute to oligomer formation. Thus, a combination of cystine noose hydrophobic interactions and complementary CM interactions may promote oligomer formation when the full-length protein is present in membrane microdomains, but peptide aggregation when the ectodomain is present by itself in an aqueous environment.

3.3. Cystine noose formation is required for liposome partitioning and lipid mixing activity

Studies suggest structural plasticity is a common feature of several enveloped viral FPs. Structural transitioning from α-helices to β-sheets has been shown for the FPs of HIV gp41, paramyxovirus F, influenza HA, and Ebola GP [51–53]. Since a high-resolution, three-dimensional structure of the p10 ectodomain was not determinable by NMR, the functional implications of the p10 disulfide bond were assessed by other means. Using far-ultraviolet CD spectroscopy, we measured the global secondary structure characteristics of ARV p10ecto under both oxidized and reduced conditions in aqueous and liposome environments (Fig. 3A). The reduced p10ecto peptide displayed nearly identical spectra in an aqueous environment and in the presence of liposomes (Fig. 3A), implying the same overall conformation under both conditions. These spectra were quite distinct from the spectra obtained for the non-reduced p10ecto peptide under both conditions (Fig. 3A). While changes in peptide solubility could contribute to changes in the CD spectra of the different peptides under different conditions, the relatively long-term (>5 h) solubility of high concentration peptide (0.5 mM) and the substantial differences in CD spectra following short-term (<1 h) incubation of low concentration peptide (0.01 mM) suggest that differences in the CD spectra at least partially reflect differences in peptide structure. Together, these results suggest that the disulfide bond induces structuring within the p10 ectodomain required either for lipid-induced structural changes in the peptide or increased lipid-mediated peptide solubility.

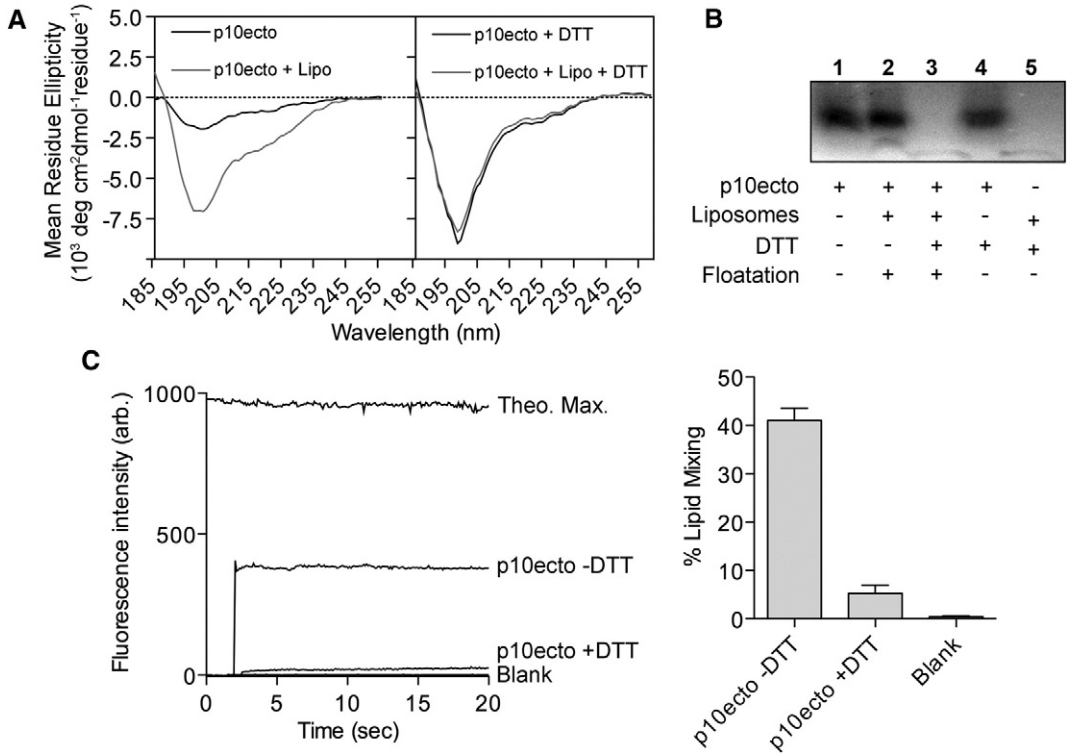

Fig. 3. An intramolecular disulfide bond is required for membrane binding and lipid mixing activity of the p10 ectodomain fusion peptide. (A) CD measurements of the ARV p10ecto synthetic peptide in aqueous and liposome conditions, with and without DTT. (B) Silver-stained tricine gel showing partitioning of the p10ecto peptide into liposomes composed of 40:30:20:10 DOPC:DOPE:Chol:Sph, in the absence (lane 2) or presence (lane 3) of DTT. Input peptide (lane 1), input peptide treated with DTT (lane 4) and liposomes treated with DTT (lane 5) are included as controls. (C) Liposome lipid mixing activity of the ARV p10ecto peptide with and without DTT showing raw fluorescence data (left) and mean +/− standard deviation of % lipid mixing from four replicates (right). Theoretical maximum fluorescence from 0.2% NBD- and Rho-labeled liposomes is shown with raw data.

To test the ability of the cystine noose to promote p10 partitioning into liposomes, ARV p10ecto in the oxidized and reduced states was mixed with liposomes and liposomes were subsequently separated from free peptide by flotation on sucrose-density gradients. The liposome-associated peptide in the liposome fraction from sucrose gradients was detected by SDS-tricine gel electrophoresis and silver staining. The oxidized ARV p10ecto peptide containing the cystine noose avidly partitioned into liposomes, and this partitioning was lost when the peptide was reduced using DTT (Fig. 3B).

ARV p10ecto was also analyzed for lipid mixing activity using a commonly employed fluorescence resonance energy transfer (FRET) based liposome assay [35]. In this assay, exogenous peptide is added to a 9:1 mixed population of unlabeled to NBD/rhodamine fluorescently-labeled liposomes (peptide:lipid ratio of 1:10). Lipid mixing between the labeled and unlabeled liposomes is detected by changes in FRET, measured as intensified NBD emission as the average spatial separation of the NBD/rhodamine FRET pair is increased upon mixing of the labeled and unlabeled liposomes. As shown (Fig. 3C), cystine noose-containing ARV p10ecto induced rapid and robust lipid mixing, while reduced versions of this peptide induced lipid mixing at levels only slightly above background. To ensure the reducing agent had no effect on the FRET assay, this assay was repeated in the absence of peptide, using increasing concentrations of Triton X-100 to induce partial liposome solubilization and lipid mixing. The presence of DTT had no effect on NBD emission (Supplementary Fig. 1). Thus, the cystine noose FP is required for p10 ectodomain partitioning into lipid bilayers and for p10-mediated lipid bilayer destabilization.

3.4. Lipid mixing occurs in the absence of detectable liposome tubulation

FPs present in protein components of the intracellular vesicle fusion machinery induce liposome-liposome fusion by generating liposome tubules with highly curved, fusogenic lipidic end caps [12,15]. A similar fusion mechanism for enveloped virus FPs has not been demonstrated. To determine whether the lipid mixing activity of the p10 ectodomain FP reflects formation of fusogenic liposome tubules, ARV and NBV p10ecto peptides (10 μM) were incubated with 100 nm liposomes composed of 40:30:20:10 DOPC:DOPE:Chol:Sph at a 1:10 peptide:lipid molar ratio, the same conditions under which lipid mixing was observed (Fig. 3C). Liposome size and morphology were examined using electron microscopy. For both the ARV and NBV peptides, there was a visible increase in the size of roughly spherical liposomes following lipid mixing but liposome tubules were undetectable by electron microscopy (Fig. 4B). The diameters of approximately 900 liposomes from two independent experiments were measured, and liposomes were binned into size classes. When analyzed as percent liposomes in each bin size, or as percent total liposome volume in each bin size, there was a clear increase in the number of liposomes in the larger bin sizes (Fig. 4A). Correspondingly, the mean liposome volume increased from 466 μm^3 for control liposomes to 739 μm^3 or 929 μm^3 for liposomes in the presence of ARV or NBV ectodomain peptide, respectively. The p10 cystine noose FP therefore induces liposome fusion in the absence of liposome tubulation.

In contrast to the extremely rapid kinetics of p10-induced lipid mixing occurring in the absence of liposome tubulation shown here, lipid mixing occurs more gradually (~several minutes) in similar FRET-based assays of tubulation-dependent liposome fusion mediated by components of intracellular vesicle fusion complexes [12,15]. One possible explanation for these differences is peptide:lipid ratios: our assays used a 1:10 ratio while tubulation and lipid mixing assays with Doc2b and the N-BAR domain of endophilin used ratios of ~1:50–1:200. However, we recently demonstrated that peptide:lipid ratios of 1:20 reduced the overall extent, but not the rate, of lipid mixing induced by the ARV and NBV p10ecto peptides [27], suggesting peptide:lipid ratios are unlikely to account for p10-induced liposome fusion in the absence of liposome tubulation. Regardless of the explanation for the

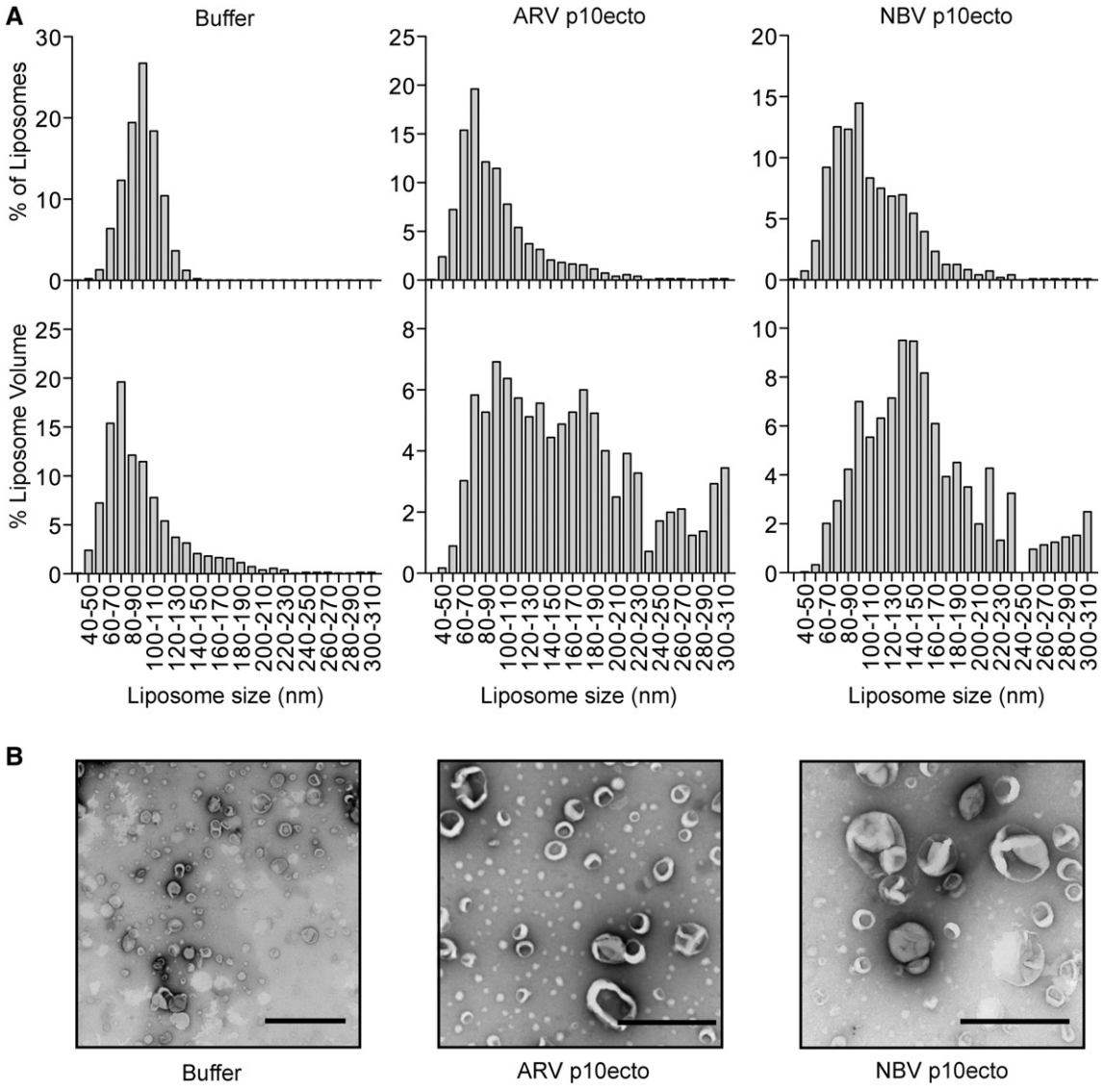

Fig. 4. The ARV and NBV p10ecto peptides induce liposome lipid mixing in the absence of liposome tubulation. (A) Liposome size distributions following ARV or NBV p10ecto peptide-induced liposome lipid mixing. Results are presented as % of total liposome counts (top) and % of total liposome volume (bottom) relative to control liposomes for each liposome diameter bin size. (B) Representative EM images of negatively-stained control liposomes and liposomes incubated with ARV p10ecto or NBV p10ecto. Scale bar = 500 nm.

different liposome fusion mechanisms employed by the p10 and cellular vesicle FPs, the p10 cystine noose FP can clearly induce liposome fusion in the absence of liposome tubulation.

3.5. Cholesterol stimulates p10 FP-induced lipid mixing

Lipid composition can have profound effects on the fusion activity of FPs. For example, Chol levels directly influence the structure and lipid mixing activity of the HIV gp41 FP [54]. We therefore assessed the lipid mixing activity of ARV p10ecto using liposomes composed of DOPC:DOPE:Chol:Sph in various molar ratios. For all experiments, the mol % of DOPE was kept constant at 30% while that of DOPC was varied with Chol or Sph, as indicated. When varying Chol, the mol % of Sph was kept at 10%. Similarly, when varying the amount of Sph, the mol % of Chol was kept at 20%. Under these various conditions, there was a substantial increase in lipid mixing as Chol content was raised from 0–10% ($P < 0.0001$) and 10–20% ($P = 0.0005$), but no statistically significant increase in lipid mixing occurred as Chol was raised from 20–30% ($P = 0.2227$, Fig. 5A). An increase in lipid mixing activity with increased mol % Chol was not observed for the low level of lipid mixing induced by the reduced ARV p10ecto peptide ($P = 0.389$, Fig. 5B), indicating that the presence of Chol does not simply alter the overall fusogenicity of the membrane. In contrast, changes in Sph content had only modest, though statistically significant, effects on p10-induced liposome fusion, which increased from 0–10% Sph ($P = 0.0007$), but decreased from 10–20% Sph ($P = 0.0034$) and 20–30% Sph ($P = 0.0007$) (Fig. 5C). Membrane fusion mediated by the p10 cystine noose FP is therefore enhanced in Chol-containing membranes.

Previous studies have shown that increasing Chol content increases the ability of the HIV gp41 FP to induce lipid mixing, which is accompanied by a structural transition from an α-helical to β-sheet conformation [54]. Such was not the case for the ARV p10ecto peptide, as indicated by the near identical CD spectra obtained in the presence of liposomes containing a 0-30 mol% range of Chol (Fig. 5D). The presence of Chol in membranes has also been implicated in the binding and insertion of the Semliki Forest virus FP into target membranes [55]. Again, such was not the case for ARV p10ecto peptide; liposome partitioning of p10ecto was unaffected by the absence of cholesterol in liposomes (Fig. 5E), assessed using the same liposome partitioning experiment previously used to show peptide partitioning into liposomes containing 20 mol% Chol (Fig. 3B). As with Chol-containing liposomes, peptide partitioning into Chol-free liposomes was dependent on the presence

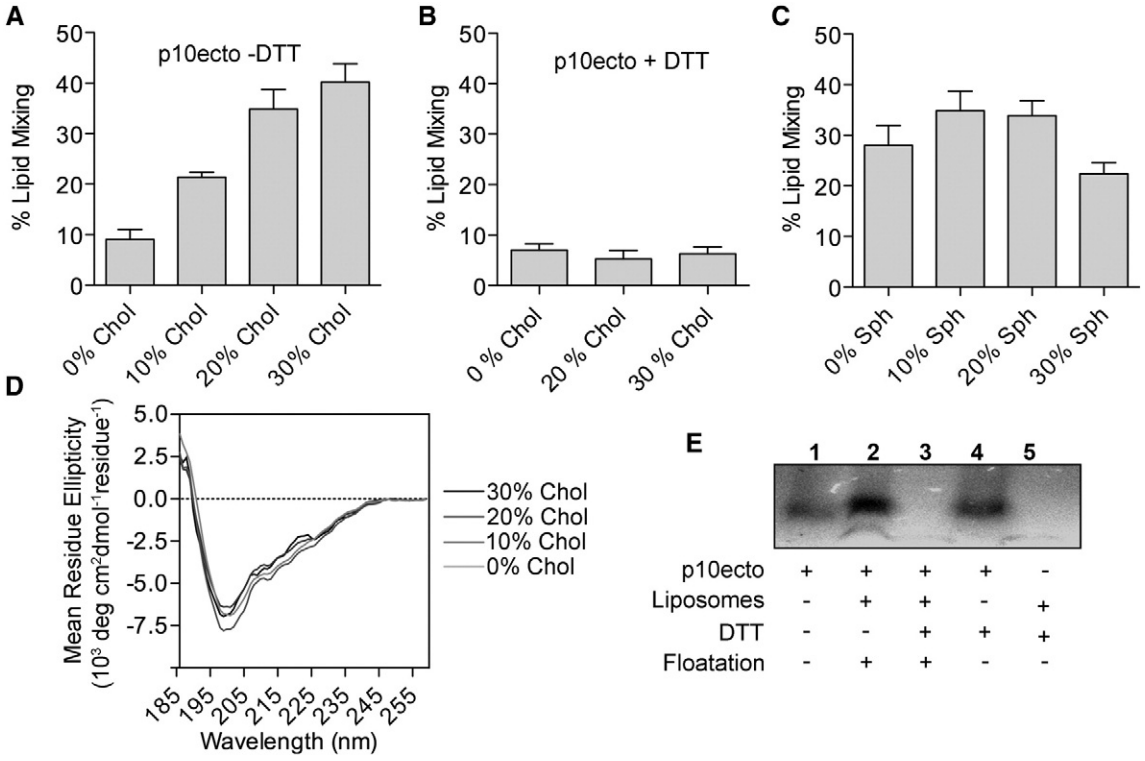

Fig. 5. Cholesterol influences the lipid mixing activity of p10ecto peptide. (A and B) Liposome lipid mixing activity of ARV p10ecto peptide in the absence (A) or presence (B) of DTT with liposomes of the indicated Chol content. (C) Liposome lipid mixing activity of ARV p10ecto peptide with liposomes of the indicated Sph content. (D) CD measurements of the ARV p10ecto peptide incubated with liposomes of varying Chol content. (E) Silver-stained tricine gel showing partitioning of the p10ecto peptide into liposomes composed of 60:30:0:10 DOPC:DOPE:Chol:Sph in the absence (lane 2) or presence (lane 3) of DTT. Input peptide (lane 1), input peptide treated with DTT (lane 4) and liposomes treated with DTT (lane 5) are included as controls.

of the cystine noose (Fig. 5E). Thus, Chol does not influence membrane partitioning of the p10 cystine noose FP, but instead has a direct influence on p10 FP-induced membrane fusion activity.

Chol may influence p10-mediated membrane fusion in several ways. As a prerequisite to lipid mixing and fusion stalk formation, two bilayers must be closely apposed. At these short separation distances, repulsive "hydration forces" dominate [56]. The presence of Chol facilitates membrane dehydration, thus promoting membrane contact and fusion [57]. The HIV gp41 and influenza virus HA FPs have been shown to increase the order of membranes in a Chol-dependent fashion, with Chol influencing the overall fusogenicity by both altering the insertion depth of FPs and maximizing the dehydration effect at the site of fusion [54,58]. Additionally, the molecular shape of Chol has been suggested to promote negative curvature in the outer bilayer leaflet [59], which can increase the formation of fusion intermediates by lowering the energy barriers of transition states. Additional studies are needed to determine whether these, or other, effects of Chol on membranes contribute to the demonstrated Chol-dependent fusion activity of the p10ecto FP.

Supplementary data to this article can be found online at http://dx.doi.org/10.1016/j.bbamem.2014.10.020.

Acknowledgements

This work was supported by a grant to R.D. from the Canadian Institutes of Health Research (CIHR). T.K. and M.S. were partially supported by a Scotia Support Grant to J.K.R. and R.D. from the Nova Scotia Health Research Foundation (NSHRF). J.K.R. is supported by a CIHR New Investigator Award.

References

[1] M. Oren-Suissa, B. Podbilewicz, Cell fusion during development, Trends Cell Biol. 17 (2007) 537–546.
[2] S.C. Harrison, Viral membrane fusion, Nat. Struct. Mol. Biol. 15 (2008) 690–698.
[3] J.M. White, S.E. Delos, M. Brecher, K. Schornberg, Structures and mechanisms of viral membrane fusion proteins: multiple variations on a common theme, Crit. Rev. Biochem. Mol. Biol. 43 (2008) 189–219.
[4] L.V. Chernomordik, M.M. Kozlov, Mechanics of membrane fusion, Nat. Struct. Mol. Biol. 15 (2008) 675–683.
[5] A.L. Lai, H. Park, J.M. White, L.K. Tamm, Fusion peptide of influenza hemagglutinin requires a fixed angle boomerang structure for activity, J. Biol. Chem. 281 (2006) 5760–5770.
[6] Y. Li, L.K. Tamm, Structure and plasticity of the human immunodeficiency virus gp41 fusion domain in lipid micelles and bilayers, Biophys. J. 93 (2007) 876–885.
[7] J.L. Lorieau, J.M. Louis, A. Bax, The complete influenza hemagglutinin fusion domain adopts a tight helical hairpin arrangement at the lipid:water interface, Proc. Natl. Acad. Sci. U. S. A. 107 (2010) 11341–11346.
[8] S.M. Gregory, E. Harada, B. Liang, S.E. Delos, J.M. White, L.K. Tamm, Structure and function of the complete internal fusion loop from Ebolavirus glycoprotein 2, Proc. Natl. Acad. Sci. U. S. A. 108 (2011) 11211–11216.
[9] Y. Modis, S. Ogata, D. Clements, S.C. Harrison, Structure of the dengue virus envelope protein after membrane fusion, Nature 427 (2004) 313–319.
[10] M.M. Kozlov, H.T. McMahon, L.V. Chernomordik, Protein-driven membrane stresses in fusion and fission, Trends Biochem. Sci. 35 (2010) 699–706.
[11] J.L. Gallop, C.C. Jao, H.M. Kent, P.J. Butler, P.R. Evans, R. Langen, H.T. McMahon, Mechanism of endophilin N-BAR domain-mediated membrane curvature, EMBO J. 25 (2006) 2898–2910.
[12] A.J. Groffen, S. Martens, R. Diez Arazola, L.N. Cornelisse, N. Lozovaya, A.P. de Jong, N.A. Goriounova, R.L. Habets, Y. Takai, J.G. Borst, N. Brose, H.T. McMahon, M. Verhage, Doc2b is a high-affinity Ca2+ sensor for spontaneous neurotransmitter release, Science 327 (2010) 1614–1618.
[13] E. Hui, C.P. Johnson, J. Yao, F.M. Dunning, E.R. Chapman, Synaptotagmin-mediated bending of the target membrane is a critical step in Ca(2+)-regulated fusion, Cell 138 (2009) 709–721.
[14] H. Yu, S.S. Rathore, E.M. Davis, Y. Ouyang, J. Shen, Doc2b promotes GLUT4 exocytosis by activating the SNARE-mediated fusion reaction in a calcium- and membrane bending-dependent manner, Mol. Biol. Cell 24 (2013) 1176–1184.
[15] S. Martens, M.M. Kozlov, H.T. McMahon, How synaptotagmin promotes membrane fusion, Science 316 (2007) 1205–1208.
[16] H. Attoui, P. Mertens, J. Becnel, S. Belaganahalli, M. Bergoin, C. Brussaard, J. Chappell, M. Ciarlet, M. del Vas, T. Dermody, P. Dormitzer, R. Duncan, Q. Fcang, R. Graham, K. Guglielmi, R. Harding, B. Hillman, A. Makkay, C. Marzachì, J. Matthijnssens, R. Milne, F. Mohd Jaafar, H. Mori, A. Noordeloos, T. Omura, J. Patton, S. Rao, M. Maan, D. Stoltz, N. Suzuki, N. Upadhyaya, C. Wei, H. Zhou, Family reoviridae, in: K. AMQ, A. MJ, C. EB, L. EJ (Eds.), Virus Taxonomy: Ninth Report of the International Committee on Taxonomy of Viruses, Elsevier/Academic Press, San Diego, USA, 2012, pp. 541–637.

[17] J. Boutilier, R. Duncan, The reovirus fusion-associated small transmembrane (FAST) proteins: virus-encoded cellular fusogens, in: L.V. Chernomordik, M.M. Koslov (Eds.), Membrane Fusion, vol. 68, Elsevier, USA, 2011, pp. 107–140.
[18] J.A. Corcoran, R. Duncan, Reptilian reovirus utilizes a small type III protein with an external myristylated amino terminus to mediate cell–cell fusion, J. Virol. 78 (2004) 4342–4351.
[19] S. Dawe, R. Duncan, The S4 genome segment of baboon reovirus is bicistronic and encodes a novel fusion-associated small transmembrane protein, J. Virol. 76 (2002) 2131–2140.
[20] H. Guo, X. Sun, L. Yan, L. Shao, Q. Fang, The NS16 protein of aquareovirus-C is a fusion-associated small transmembrane (FAST) protein, and its activity can be enhanced by the nonstructural protein NS26, Virus Res. 171 (2013) 129–137.
[21] T. Racine, T. Hurst, C. Barry, J. Shou, F. Kibenge, R. Duncan, Aquareovirus effects syncytiogenesis by using a novel member of the FAST protein family translated from a noncanonical translation start site, J. Virol. 83 (2009) 5951–5955.
[22] M. Shmulevitz, R. Duncan, A new class of fusion-associated small transmembrane (FAST) proteins encoded by the non-enveloped fusogenic reoviruses, EMBO J. 19 (2000) 902–912.
[23] C.M. Thalmann, D.M. Cummins, M. Yu, R. Lunt, L.I. Pritchard, E. Hansson, S. Crameri, A. Hyatt, L.F. Wang, Broome virus, a new fusogenic Orthoreovirus species isolated from an Australian fruit bat, Virology 402 (2010) 26–40.
[24] C. Barry, T. Key, R. Haddad, R. Duncan, Features of a spatially constrained cystine loop in the p10 FAST protein ectodomain define a new class of viral fusion peptide, J. Biol. Chem. 285 (2010) 16424–16433.
[25] J.A. Corcoran, R. Syvitski, D. Top, R.M. Epand, R.F. Epand, D. Jakeman, R. Duncan, Myristoylation, a protruding loop, and structural plasticity are essential features of a nonenveloped virus fusion peptide motif, J. Biol. Chem. 279 (2004) 51386–51394.
[26] D. Top, J.A. Read, S.J. Dawe, R.T. Syvitski, R. Duncan, Cell–cell membrane fusion induced by p15 fusion-associated small transmembrane (FAST) protein requires a novel fusion peptide motif containing a myristoylated polyproline type II helix, J. Biol. Chem. 287 (2012) 3403–3414.
[27] T. Key, R. Duncan, A compact, multifunctional fusion module directs cholesterol-dependent homomultimerization and syncytiogenic efficiency of reovirus p10 FAST proteins, PLoS Pathog. 10 (2014) e1004023.
[28] D.L. Gibbons, M.C. Vaney, A. Roussel, A. Vigouroux, B. Reilly, J. Lepault, M. Kielian, F.A. Rey, Conformational change and protein–protein interactions of the fusion protein of Semliki Forest virus, Nature 427 (2004) 320–325.
[29] S.F. Cheng, C.W. Wu, E.A. Kantchev, D.K. Chang, Structure and membrane interaction of the internal fusion peptide of avian sarcoma leukosis virus, Eur. J. Biochem. 271 (2004) 4725–4736.
[30] S.E. Delos, J.M. White, Critical role for the cysteines flanking the internal fusion peptide of avian sarcoma/leukosis virus envelope glycoprotein, J. Virol. 74 (2000) 9738–9741.
[31] M.S. Freitas, L.P. Gaspar, M. Lorenzoni, F.C. Almeida, L.W. Tinoco, M.S. Almeida, L.F. Maia, L. Degreve, A.P. Valente, J.L. Silva, Structure of the Ebola fusion peptide in a membrane-mimetic environment and the interaction with lipid rafts, J. Biol. Chem. 282 (2007) 27306–27314.
[32] J.E. Lee, M.L. Fusco, A.J. Hessell, W.B. Oswald, D.R. Burton, E.O. Saphire, Structure of the Ebola virus glycoprotein bound to an antibody from a human survivor, Nature 454 (2008) 177–182.
[33] A.J. Lapthorn, R.W. Janes, N.W. Isaacs, B.A. Wallace, Cystine nooses and protein specificity, Nat. Struct. Biol. 2 (1995) 266–268.
[34] M.L. Tremblay, A.W. Banks, J.K. Rainey, The predictive accuracy of secondary chemical shifts is more affected by protein secondary structure than solvent environment, J. Biomol. NMR 46 (2010) 257–270.
[35] D.K. Struck, D. Hoekstra, R.E. Pagano, Use of resonance energy transfer to monitor membrane fusion, Biochemistry 20 (1981) 4093–4099.
[36] L.T. Cheng, R.K. Plemper, R.W. Compans, Atypical fusion peptide of Nelson Bay virus fusion-associated small transmembrane protein, J. Virol. 79 (2005) 1853–1860.
[37] M. Shmulevitz, R.F. Epand, R.M. Epand, R. Duncan, Structural and functional properties of an unusual internal fusion peptide in a nonenveloped virus membrane fusion protein, J. Virol. 78 (2004) 2808–2818.
[38] G.V. Semisotnov, N.A. Rodionova, O.I. Razgulyaev, V.N. Uversky, A.F. Gripas, R.I. Gilmanshin, Study of the "molten globule" intermediate state in protein folding by a hydrophobic fluorescent probe, Biopolymers 31 (1991) 119–128.
[39] F. Chiti, M. Stefani, N. Taddei, G. Ramponi, C.M. Dobson, Rationalization of the effects of mutations on peptide and protein aggregation rates, Nature 424 (2003) 805–808.
[40] A.P. Pawar, K.F. DuBaya, J. Zurdoa, F. Chitib, M. Vendruscoloa, C.M. Dobsona, Prediction of "aggregation-prone" and "aggregation-susceptible" regions in proteins associated with neurodegenerative diseases, J. Mol. Biol. 350 (2005) 379–392.
[41] M. Pannuzzo, A. Raudino, D. Milardi, C. La Rosa, M. Karttunen, alpha-helical structures drive early stages of self-assembly of amyloidogenic amyloid polypeptide aggregate formation in membranes, Sci. Rep. 3 (2013) 2781.
[42] I. Sepkhanova, M. Drescher, N.J. Meeuwenoord, R.W.A.L. Limpens, R.I. Koning, D.V. Filippov, M. Huber, Monitoring alzheimer amyloid peptide aggregation by EPR, Appl. Magn. Reson. 36 (2009) 2–4.
[43] J.M. Andreu, S.N. Timasheff, The measurement of cooperative protein self-assembly by turbidity and other techniques, Methods Enzymol. 130 (1986) 47–59.
[44] S.I.A. Cohen, M. Vendruscolo, C.M. Dobson, T.P.J. Knowles, From macroscopic measurements to microscopic mechanisms of protein aggregation, J. Mol. Biol. 421 (2012) 160–171.
[45] M. Shmulevitz, J. Corcoran, J. Salsman, R. Duncan, Cell–cell fusion induced by the avian reovirus membrane fusion protein is regulated by protein degradation, J. Virol. 78 (2004) 5996–6004.
[46] J. Cavanagh, W.J. Fairbrother, A.G. Palmer, M. Rance, N.J. Skelton, Protein NMR spectroscopy: principles and practice, 2nd ed. Elsevier Academic Press, San Diego, USA, 2007.
[47] A. Abelein, B. Bolognesi, C.M. Dobson, A. Graslund, C. Lendel, Hydrophobicity and conformational change as mechanistic determinants for nonspecific modulators of amyloid ß self-assembly, Biochemistry 51 (2012) 126–137.
[48] A.S. Maltsev, A. Grishaev, A. Bax, Monomeric alpha-synuclein binds Congo red micelles in a disordered manner, Biochemistry 51 (2012) 631–642.
[49] A. Wahlström, L. Hugonin, A. Peralvarez-Marin, J. Jarvet, A. Gräslund, Secondary structure conversions of Alzheimer's Aß(1–40) peptide induced by membrane-mimicking detergents, FEBS J. 275 (2008) 5117–5128.
[50] D.S. Wishart, B.D. Sykes, F.M. Richards, The chemical shift index — a fast and simple method for the assignment of protein secondary structure through NMR-spectroscopy, Biochemistry 31 (1992) 1647–1651.
[51] K. Sackett, M.J. Nethercott, R.F. Epand, R.M. Epand, D.R. Kindra, Y. Shai, D.P. Weliky, Comparative analysis of membrane-associated fusion peptide secondary structure and lipid mixing function of HIV gp41 constructs that model the early pre-hairpin intermediate and final hairpin conformations, J. Mol. Biol. 397 (2010) 301–315.
[52] A. Agopian, S. Castano, Structure and orientation study of Ebola fusion peptide inserted in lipid membrane models, Biochim. Biophys. Acta 1838 (2014) 117–126.
[53] X. Han, L.K. Tamm, pH-dependent self-association of influenza hemagglutinin fusion peptides in lipid bilayers, J. Mol. Biol. 304 (2000) 953–965.
[54] A.L. Lai, A.E. Moorthy, Y. Li, L.K. Tamm, Fusion activity of HIV gp41 fusion domain is related to its secondary structure and depth of membrane insertion in a cholesterol-dependent fashion, J. Mol. Biol. 418 (2012) 3–15.
[55] A. Ahn, D.L. Gibbons, M. Kielian, The fusion peptide of Semliki Forest virus associates with sterol-rich membrane domains, J. Virol. 76 (2002) 3267–3275.
[56] S. Leikin, V.A. Parsegian, D.C. Rau, Hydration forces, Annu. Rev. Phys. Chem. 44 (1993) 369–395.
[57] S. Aeffner, T. Reusch, B. Weinhausen, T. Salditt, Energetics of stalk intermediates in membrane fusion are controlled by lipid composition, Proc. Natl. Acad. Sci. U. S. A. 109 (2012) E1609–E1618.
[58] A.L. Lai, J.H. Freed, HIV gp41 fusion peptide increases membrane ordering in a cholesterol-dependent fashion, Biophys. J. 106 (2014) 172–181.
[59] Z. Chen, R.P. Rand, The influence of cholesterol on phospholipid membrane curvature and bending elasticity, Biophys. J. 73 (1997) 267–276.